The difficulty for subducted oceanic crust to accumulate at the Earth's core-mantle boundary

Mingming Li[1] and Allen K. McNamara[1]

Received 10 September 2012; revised 4 March 2013; accepted 7 March 2013.

[1] Seismic tomography has revealed two large low shear velocity provinces (LLSVPs) in the lowermost mantle beneath the central Pacific and Africa. The LLSVPs are further shown to be compositionally different from their surroundings. Among several hypotheses put forth in recent years to explain the cause of the LLSVPs, one postulates that they are thermochemical piles caused by accumulation of subducted oceanic crust at the core-mantle boundary (CMB). Mineral physics experiments indicate that oceanic crust becomes denser than the surrounding mantle at lower mantle pressures. In addition, seismic observations provide evidence of subducted slabs arriving at the CMB. However, a major question pertains to whether subducted oceanic crust can survive viscous stirring associated with mantle plumes and accumulate into piles with the same spatial scale as LLSVPs. We perform a set of high-resolution convection calculations to examine this hypothesis by investigating the interaction of thin oceanic crust (6 km) with mantle plumes. Our results show that as subducted oceanic crust is swept toward upwelling plume regions, the majority of it is viscously stirred into the surrounding mantle. Only a small amount of oceanic crust may accumulate at the base of plumes, but it is consistently entrained away into the plume at a rate equal to or greater than it is accumulated. We find that it is difficult for subducted oceanic crust to accumulate into large thermochemical piles at the CMB.

Citation: Li, M., and A. K. McNamara (2013), The difficulty for subducted oceanic crust to accumulate at the Earth's core-mantle boundary, *J. Geophys. Res. Solid Earth*, *118*, doi:10.1002/jgrb.50156.

1. Introduction

[2] Understanding the role that compositional heterogeneity plays in controlling mantle dynamics, and therefore heat transport and thermal evolution, remains one of the most challenging problems in Earth science. A critical question relates to the origin and dynamic nature of the proposed large-scale compositional heterogeneity in the Earth's lower mantle. Although it has long been proposed that the lowermost mantle of the Earth is compositionally heterogeneous on a global scale [e.g., *Masters et al*., 2000; *Trampert et al*., 2004], the cause of this heterogeneity and how it affects mantle dynamics are not well understood.

[3] Seismic tomography studies have discovered the existence of two large low shear velocity provinces (LLSVPs) in the lowermost mantle beneath the central Pacific and Africa [e.g., *Li and Romanowicz*, 1996; *Su and Dziewonski*, 1997; *Grand*, 2002; *Ritsema et al*., 2004]. These are regions furthest removed from paleosubduction, and geodynamical studies have revealed that the Earth's subduction history should act to drive upwellings in these regions [*Bunge et al*., 1998; *Zhong et al*., 2000; *McNamara and Zhong*, 2005]. The two LLSVP anomalies beneath Africa and the central Pacific are both of large size. As demonstrated in recent seismic studies, the African anomaly may be a single massive pile reaching 1300 km above the core-mantle boundary (CMB), and the Pacific anomaly may contain several piles whose height ranges from ~400 km to at least 740 km [*Wang and Wen*, 2007; *He and Wen*, 2009; *He and Wen*, 2012]. Interestingly, paleomagnetic constraints infer that the LLSVPs may have been in their current locations for several hundred million years [e.g., *Torsvik et al*., 2010]. The LLSVPs are also characterized by increased density [e.g., *Ishii and Tromp*, 1999; *Trampert et al*., 2004], large d ln *Vs*/d ln *Vp* ratio [e.g., *Wang and Wen*, 2007], and anticorrelation between seismic shear velocity and bulk sound speed [*Trampert et al*., 2004]. In addition, seismic traveltime and waveform studies indicate sharp edges [e.g., *Wen*, 2001; *Wen et al*., 2001] and large contrasts in elastic properties within the LLSVP regions, particularly along the margins [e.g., *Ni et al*., 2002; *Ni and Helmberger*, 2003; *Wang and Wen*, 2004; *To et al*., 2005; *Ford et al*., 2006; *He and Wen*, 2009].

[4] The characteristics of the LLSVPs discussed above suggest that their composition is different from that of the background mantle [e.g., *Ishii and Tromp*, 1999; *Masters et al*., 2000; *Trampert et al*., 2004; *Hernlund and Houser*, 2008]. Possible origins for a distinct composition of LLSVPs may include (1) products resulting from the interaction between the mantle and core [e.g., *Buffett et al*., 2000;

[1]School of Earth and Space Exploration, Arizona State University, Tempe, Arizona, USA.

Corresponding author: M. Li, School of Earth and Space Exploration, Arizona State University, PO Box 871404, Tempe, AZ 85287-1404, USA. (Mingming.Li@asu.edu)

2169-9313/13/10.1002/jgrb.50156

Kanda and Stevenson, 2006], (2) remnants of primordial dense reservoirs formed by differentiation in the Earth's early history [e.g., *Wen*, 2001; *Wen et al*., 2001; *Labrosse et al*., 2007; *Lee et al*., 2010; *Nomura et al*., 2011], and (3) accumulation of subducted oceanic crust at the CMB [e.g., *Christensen and Hofmann*, 1994; *Brandenburg and van Keken*, 2007; *Nakagawa et al*., 2009; *Tackley*, 2011]. Each of these possibilities is related to different dynamics and the Earth's chemical evolution [*Wen*, 2001; *Wen et al*., 2001; *Garnero and McNamara*, 2008; *Tackley*, 2012].

[5] In this study, we test the third possibility using numerical modeling. Seismic tomography shows that subducted lithosphere is able to reach the lowermost mantle [e.g., *Grand et al*., 1997; *Li et al*., 2008]. In addition, mineral physics experiments indicate that oceanic crust becomes denser than the surrounding mantle at lower mantle pressures [e.g., *Hirose et al*., 2005]. Furthermore, geodynamical experiments reveal that oceanic crust can delaminate from oceanic lithosphere in the lowermost mantle [e.g., *Tackley*, 2011]. However, an important question is whether subducted oceanic crust can survive vigorous stirring associated with mantle plumes and accumulate into large thermochemical piles with the same spatial scale as LLSVPs. The fact that oceanic crust becomes denser than the surrounding mantle at lower mantle pressures would support this idea; however, because oceanic crust is so thin compared to mantle-scale convection, it may not be able to survive viscous stirring (i.e., viscous forces dominate buoyancy forces). We investigate this question here by performing high-resolution mantle convection calculations that include realistic, 6 km, crustal thickness. We investigate whether oceanic crust can accumulate in significant quantities in upwelling plume regions over billion year timescales.

[6] Previous numerical calculations have been conducted to explore the possibility of subducted oceanic crust to accumulate at the CMB [e.g., *Christensen and Hofmann*, 1994; *Brandenburg and van Keken*, 2007; *Huang and Davies*, 2007; *Nakagawa et al.*, 2009; *Tackley*, 2011]. *Christensen and Hofmann* [1994] modeled the process of segregation and accumulation of subducted oceanic crust at the CMB. They found that of the order of one sixth of the subducted crust accumulated in pools at the bottom of the model, which resides underneath thermal plumes. In their study, the thickness of the oceanic crust is about 30 km and the Rayleigh number is moderately low because of computational limitation. Later, *Brandenburg and van Keken* [2007] expanded the results of *Christensen and Hofmann* [1994] by studying models with more Earth-like vigor. Their results show that significant accumulation is still possible at high Rayleigh number, but only when the excess density of oceanic crust in the lower mantle is larger than that currently suggested from laboratory experiments. *Huang and Davies* [2007] showed the ability of subducted oceanic crust to accumulate at the CMB using three-dimensional (3-D) calculations in which the mantle is only heated within and zero heat flux is employed at the CMB. As a result, plumes are suppressed in their study. By incorporating self-consistently calculated mineral physics into mantle convection models, *Nakagawa et al*. [2009] found that a large amount of subducted dense materials accumulate at the CMB. However, they state that they assume more mid-ocean ridge basalt (MORB) material in the petrological model, which explains why their calculations produce a much thicker layer of segregated MORB above the CMB. Most recently, *Tackley* [2011] simulated the process of segregating subducted oceanic crust from a compositionally stratified slab in both two-dimensional (2-D) and three-dimensional (3-D) models. The results show that a large fraction of subducted oceanic crust can segregate and remain at the CMB if a primordial dense layer exists at the lowermost mantle. However, the thickness of the oceanic crust in his study is 30 km.

[7] It is not understood whether realistic thin 6 km oceanic crust could survive vigorous entrainment from plumes and accumulate into large piles at the CMB. In this study, we test the possibility of accumulating large amount of subducted oceanic crust at the CMB in the existence of upwelling plumes. Our calculations are featured by high resolution which allows us to study the subduction and accumulation of a realistic thin oceanic crust (6 km).

2. Method

[8] We conducted geodynamic calculations by solving the following nondimensional equations for conservation of mass, momentum, and energy using Boussinesq approximation:

$$\nabla\cdot\vec{u} = 0 \tag{1}$$

$$-\nabla P + \nabla\cdot\left(\eta\dot{\bar{\bar{\varepsilon}}}\right) = Ra(T - BC)\hat{z} \tag{2}$$

$$\frac{\partial T}{\partial t} + \left(\vec{u}\cdot\nabla\right)T = \nabla^2 T + Q \tag{3}$$

[9] Here, $\vec{u}$ is the velocity, P is the dynamic pressure, η is the viscosity, $\dot{\bar{\bar{\varepsilon}}}$ is the strain rate tensor, T is the temperature, C is the composition, $\hat{z}$ is the unit vector in the vertical direction, t is the time, and Q is the internal heating. The thermal Rayleigh number Ra is defined as

$$Ra = \frac{\rho_0 g \alpha_0 \Delta T h^3}{\eta_0 \kappa_0}$$

where ρ_0, α_0, ΔT, η_0, and κ_0 are the dimensional reference values of density, thermal expansivity, temperature difference between the CMB and surface, reference viscosity at temperature $T = 0.5$ (nondimensional), and thermal diffusivity, respectively. The g and h are the dimensional gravitational acceleration and thickness of the mantle, respectively.

[10] The chemical density anomaly is measured by buoyancy number B, which is defined as

$$B = \frac{\Delta\rho}{\rho_0 \alpha_0 \Delta T}$$

where $\Delta\rho$ is the dimensional density contrast between the oceanic crust and background mantle.

[11] All boundaries have free-slip velocity boundary conditions. The temperature boundary conditions are isothermal on the top and bottom and insulating on the sides. In this study, we examine the dynamical relationship between plumes and subducted oceanic crust, so by trial and error, we established a long-lived stable convection configuration which contains downwellings surrounded by upwelling regions on both sides. To develop an appropriate initial condition, we first performed a series of isochemical calculations to find the model with stable downwellings between two

Table 1. Cases Used in This Study[a]

Case	B	Ra	A	Q_{crust}	μ_{ppv}	Aspect Ratio	Figures
1	0.8	10^7	6.91	0	1.0	6	Figure 1
2	**0.6**	10^7	6.91	0	1.0	6	Figures 2a and 2b
3	**1.0**	10^7	6.91	0	1.0	6	Figures 2c and 2d
4	**1.2**	10^7	6.91	0	1.0	6	Figures 3a and 3b
5	**1.5**	10^7	6.91	0	1.0	6	Figures 3c and 3d
6	0.8	$\mathbf{5 \times 10^6}$	6.91	0	1.0	6	Figure 4a
7	0.8	$\mathbf{5 \times 10^7}$	6.91	0	1.0	6	Figure 4b
8	0.8	10^7	**9.21**	0	1.0	6	Figure 5
9	0.8	10^7	6.91	**20**	1.0	6	Figure 6
10	0.8	10^7	6.91	0	**0.01**	6	Figure 7
11	0.8	10^7	6.91	0	1.0	**7**	Figure 8

[a]B: Buoyancy number; Ra: Rayleigh number; A: activation parameter for temperature-dependent viscosity; Q_{crust}: internal heating for subducted oceanic crust; μ_{ppv}: viscosity contrast between post-Perovskite and Perovskite. Numbers in bold are the different parameters in each case from Case 1.

upwellings. After finding one, we ran the calculation until it reached a steady thermal state. Then, we interpolated to a high-resolution mesh and introduced about 6 million tracers to represent the compositional field.

[12] Compositional advection is performed using the ratio tracer method [*Tackley and King*, 2003]. On average, each element has 20 randomly distributed tracers which are advected with mantle flow. To provide a constant oceanic crust at the surface, we prescribe a composition of 1 to tracers that reach the upper 6 km of the model. As noted in *Christensen and Hofmann* [1994], we also found that some crustal tracers become artificially trapped to the side boundaries, which overemphasize the amount of crustal material that accumulates in the lowermost mantle because it descends directly into the lowermost thermal boundary

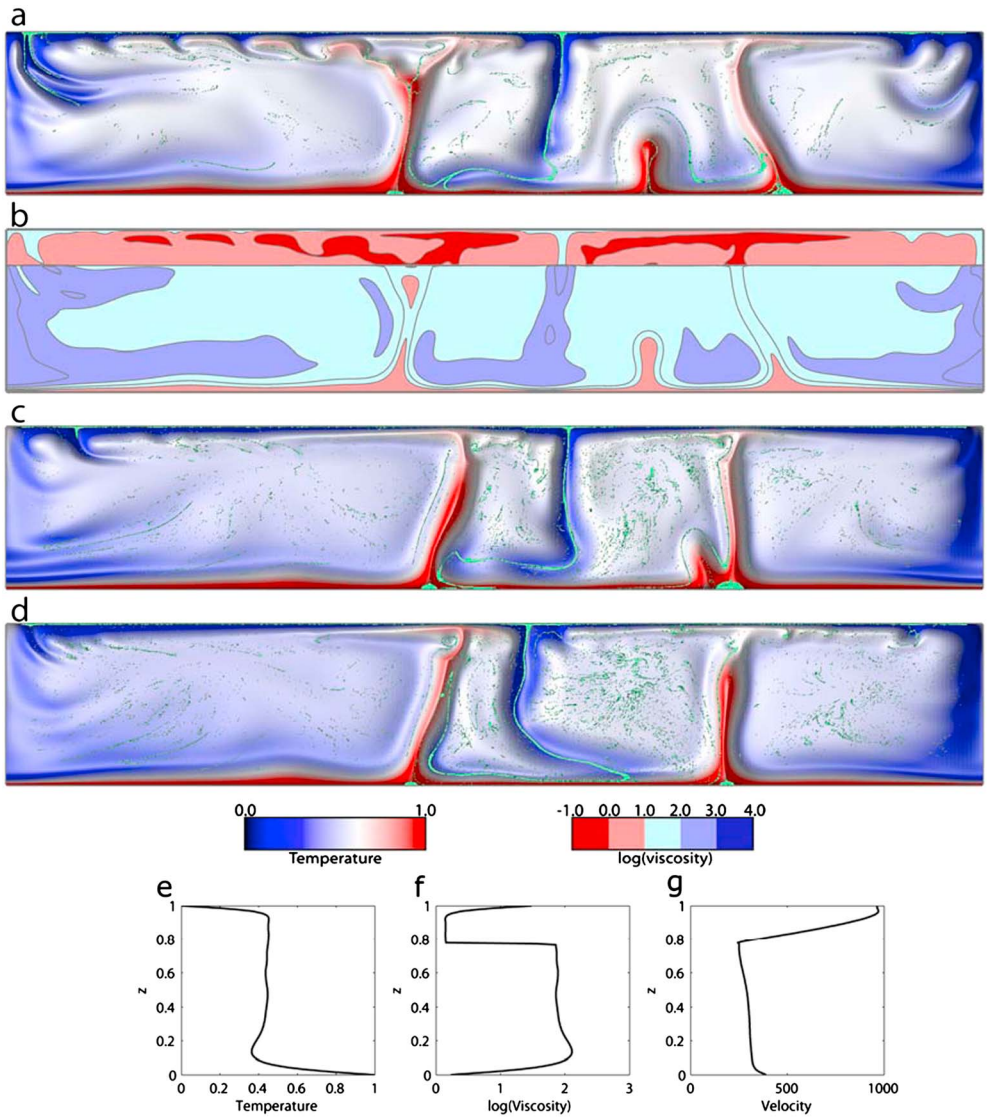

Figure 1. Case 1. (a) Snapshot (at 1.0 Gyr) of the nondimensional temperature field with oceanic crust superimposed (shown in green). (b) Logarithm of nondimensional viscosity at 1.0 Gyr. The black lines are contours of viscosity with an interval of 0.5. (c) Nondimensional temperature and oceanic crust at 2.0 Gyr. (d) Nondimensional temperature and oceanic crust at 2.8 Gyr. Profiles of (e) horizontally averaged nondimensional temperature, (f) logarithm of nondimensional viscosity, and (g) magnitude of nondimensional velocity at 1.0 Gyr. This is the reference case.

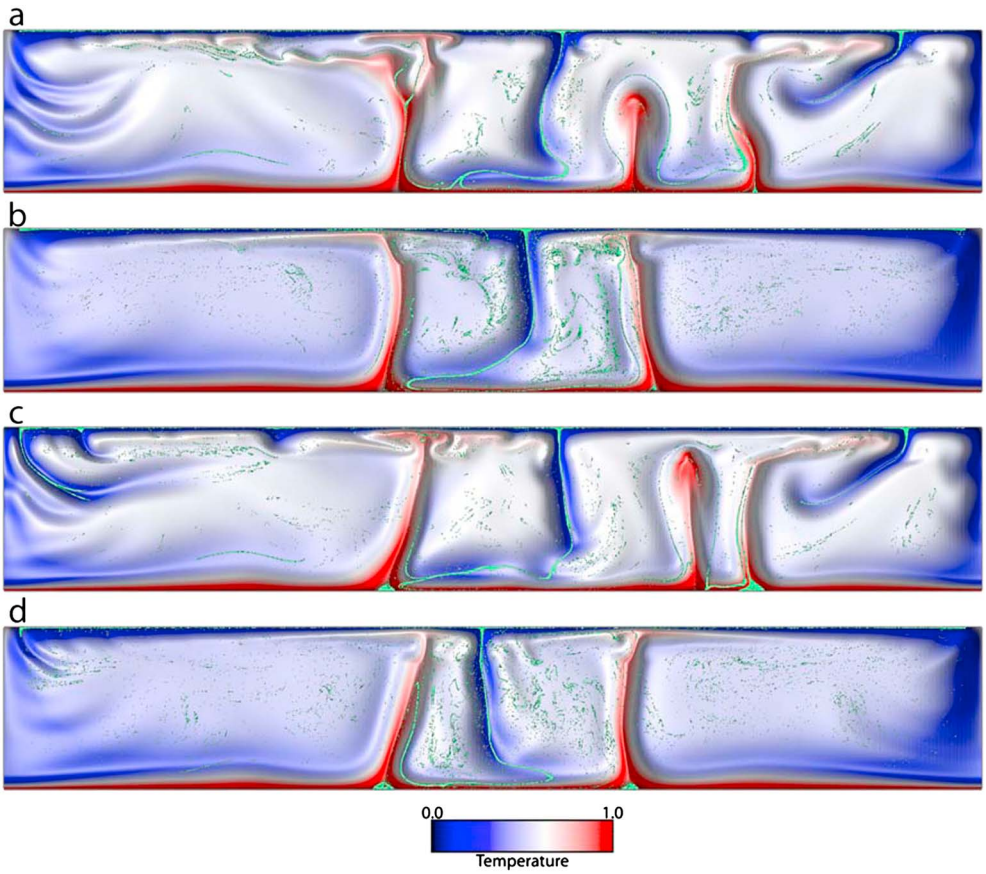

Figure 2. Snapshots of the nondimensional temperature and oceanic crust for (a, b) Case 2 and (c, d) Case 3 at 1.0 Gyr in Figures 2a and 2c and 2.8 Gyr in Figures 2b and 2d. The buoyancy number is $B = 0.6$ for Case 2 and $B = 1.0$ for Case 3.

layer. To avoid this problem, on the upper half of the model, crustal tracers are reverted back to normal background mantle if they enter a thin buffer width of 0.1 from the side boundaries. In other words, we ignore the crust that is subducted along the side boundaries of the domain to avoid artificial accumulation of crust in the lowermost mantle.

[13] *O'Farrell and Lowman* [2010] found that it is appropriate to disregard internal heating in Cartesian models in order to better simulate temperature conditions within spherical models that do include internal heating. In other words, adding internal heating to Cartesian models will overheat them and, as a consequence, suppress plume formation. Our previous experience with both spherical and Cartesian mantle convection modeling supports this idea, and we arrive at the same general conclusion as *O'Farrell and Lowman* [2010]. Therefore, we exclude internal heating for most of our cases except Case 9 in which we employ internal heating to the subducted oceanic crust to explore how this affects our results.

[14] The Perovskite to post-Perovskite phase transition is expected to form in relatively cooler portions of the lowermost mantle [e.g., *Murakami et al*., 2004; *Oganov and Ono*, 2004; *Tsuchiya et al*., 2004; *Hernlund et al*., 2005]. It is possible that the post-Perovskite phase could be less viscous than the background mantle by about 5–1000 times [e.g., *Hunt et al*., 2009; *Ammann et al*., 2010]. We investigate this possibility in Case 10 by decreasing the viscosity of post-Perovskite by 2 orders. The phase transition is expected to experience a double crossing in downwelling regions [e.g., *Hernlund et al*., 2005] which has possibly been observed by seismology [e.g., *van der Hilst et al*., 2007]. We found that the following nondimensional depth-temperature relationship produces double crossings of the transition within lowermost mantle portions of the downwellings:

$$D = T + 0.5$$

where D is the nondimensional depth and T is the nondimensional temperature. We use this relation as phase boundary between Perovskite and post-Perovskite, and we modify viscosity in post-Perovskite regions.

[15] Viscosity is a function of temperature, depth, and Perovskite/post-Perovskite phase:

$$\eta = \eta_{660}\eta_{\mathrm{ppv}} \exp[A(0.5 - T)]$$

where A and T are the activation parameter for temperature dependence of viscosity and the nondimensional temperature, respectively. The viscosity contrast due to temperature can be computed by $\Delta\eta_T = \exp(A)$. η_{660} represents the viscosity increase at the 660 km discontinuity. In all cases of this study, $\eta_{660} = 50$, indicating a 50 times viscosity increase from the upper mantle to the lower mantle across the 660 km depth [e.g., *LithgowBertelloni and Gurnis*, 1997]. η_{ppv} represents

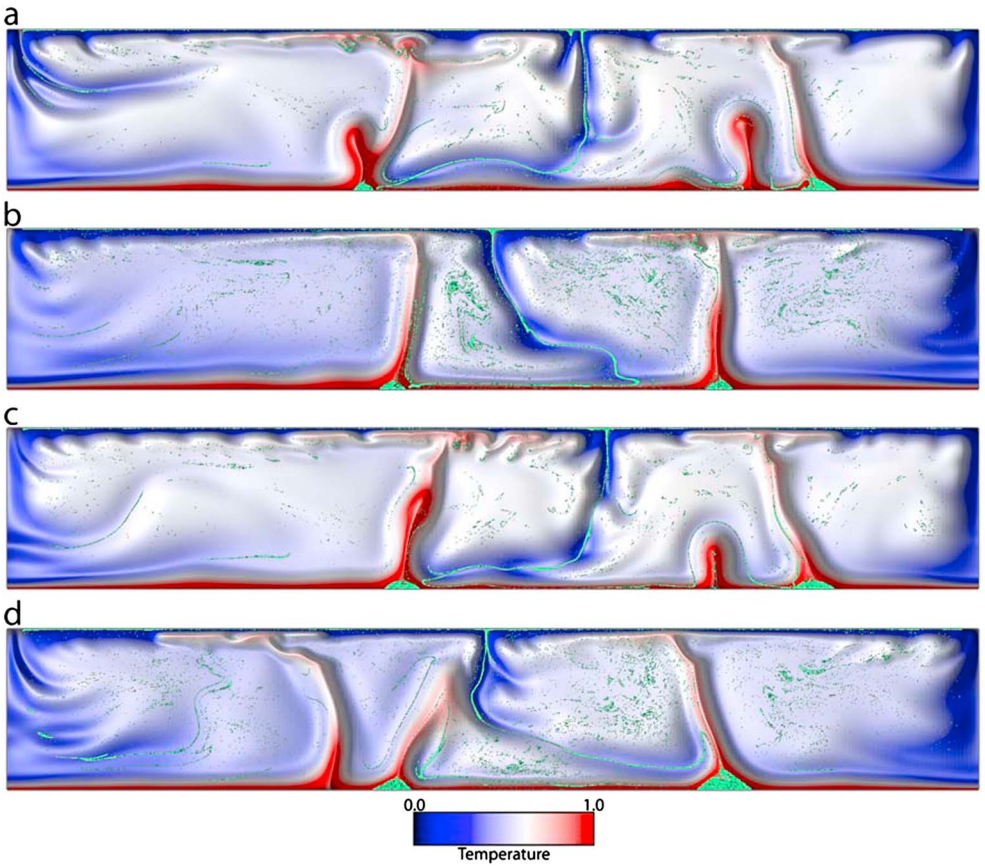

Figure 3. Snapshots of the nondimensional temperature and oceanic crust for (a, b) Case 4 and (c, d) Case 5 at 1.0 Gyr in Figures 3a and 3c and 2.8 Gyr in Figures 3b and 3d. The buoyancy number is $B = 1.2$ for Case 4 and $B = 1.5$ for Case 5.

the prescribed viscosity decrease for post-Perovskite phase transition (for Case 10).

[16] All cases are performed in 2-D Cartesian geometry. We employed an aspect ratio of 6 for all cases except Case 11, for which the aspect ratio is 7. There are 1152 and 256 elements in the horizontal and vertical directions, respectively (1344 × 256 elements for Case 11). The grid is refined in the top 6 km and bottom 600 km, resulting in resolutions of 3 km and 6 km in these regions, respectively.

[17] To solve the conservation equations, we use our modified version of the convection code, Citcom [*Moresi and Solomatov*, 1995; *Moresi and Gurnis*, 1996], that includes the thermochemical convection and composition-dependent rheology.

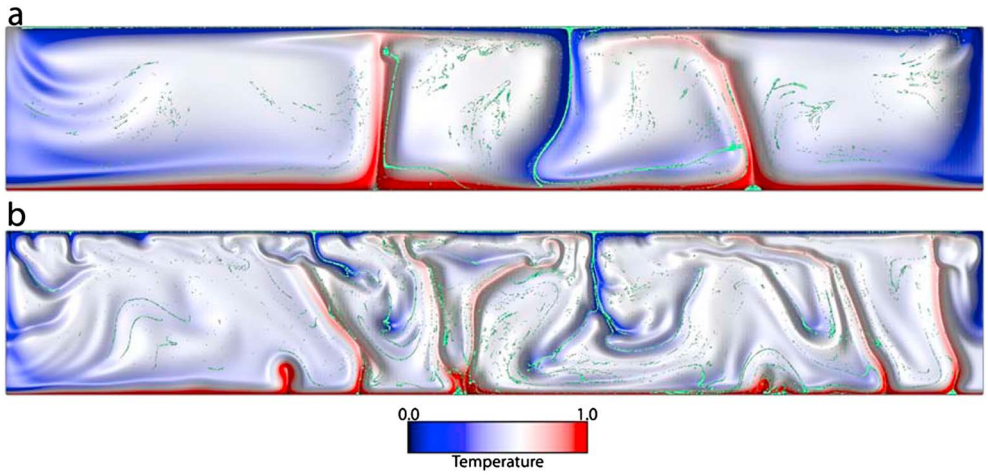

Figure 4. Snapshots (at 1.0 Gyr) of the nondimensional temperature and oceanic crust for (a) Case 6 and (b) Case 7. The Rayleigh number is $Ra = 5e6$ for Case 6 and $Ra = 5e7$ for Case 7.

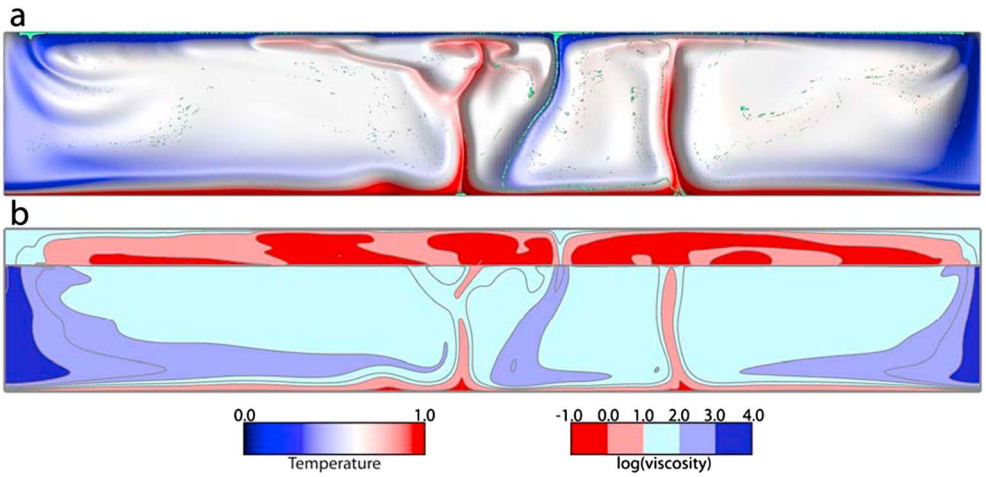

Figure 5. Case 8. (a) Snapshot (at 1.0 Gyr) of the nondimensional temperature and oceanic crust. (b) Logarithm of nondimensional viscosity at 1.0 Gyr. The black lines are contours of viscosity with an interval of 0.5. This case employs temperature dependence of viscosity 10× higher than that of the reference case.

[18] We perform the calculations for about 50 slab transit times, equating to several billion years of geologic time. Dimensionalized model time is often not that useful for timing geologic events because it is highly sensitive to accurately representing the viscosity structure, and hence effective Rayleigh number, of the actual Earth. In other words, modest uncertainties in viscosity lead to large uncertainties associated with using dimensional time to reference geologic time. Instead, for problems such as this one, it is more appropriate to reference the transit time that takes for a slab to descend to the lowermost mantle, based on surface velocity and mantle thickness. We use the following transit time scaling law, from *Christensen and Hofmann* [1994], to calculate the geological time:

$$t_G = t u_0 t^*$$

[19] where t_G is the geological time and t and u_0 are the nondimensional time and the average nondimensional surface velocity at the surface, respectively. The t^* is the transit time, which is given by $t^* = h_M/u_P$, where h_M is the thickness of the mantle and u_P is a representative mean plate velocity for the Earth. We use a transition time of 60 Ma in this study.

3. Results

[20] Here, we describe 11 representative cases (Table 1). All cases have a thin, 6 km thick crust and an intrinsic 50× viscosity increase from the upper mantle to the lower mantle (in addition to temperature-dependent viscosity). In Case 1–Case 5, the density of oceanic crust is varied. The effects of different Rayleigh numbers are explored in Case 6 and Case 7. The temperature dependence of viscosity is increased in Case 8. In Case 9, we employ internal heating to the subducted oceanic crust. Case 10 investigates a viscosity softening due to post-Perovskite in high-pressure, cooler regions [e.g., *van der Hilst et al*., 2007]. In Case 11, we choose a different aspect ratio for the model. In order to be consistent with experimental and theoretical results [*Ringwood*, 1990; *Hirose et al*., 2005; *Nakagawa et al*., 2009; *Ricolleau et al*., 2010], the buoyancy number of oceanic crust in all cases is kept in the range of 0.6–1.5 which is equivalent to a density increase of about 1.0–4.5% (depending on parameters used for nondimensionalization) for oceanic crust with respect to the background mantle.

[21] We define Case 1 as the reference case, in which the buoyancy number is 0.8 and we use an activation parameter of $A = 6.91$ for the temperature-dependent viscosity, which leads to a maximum of 1000× viscosity contrast due to temperature. The Rayleigh number for this case is $Ra = 1.0 \times 10^7$. The steady state, initial condition features a downwelling region in the middle of the domain, surrounded by upwelling plume regions on both sides of it. Oceanic crust is continuously introduced in the upper 6 km of the model, and most of which is ultimately subducted into the center downwelling region. Figure 1a illustrates the combined temperature and compositional field after 1.0 billion years of model time. Note

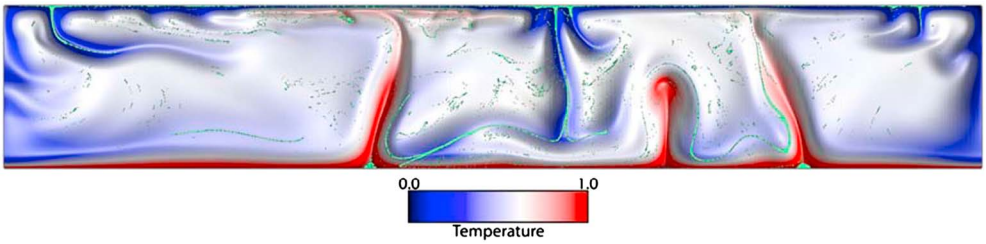

Figure 6. Snapshot of the nondimensional temperature and oceanic crust for Case 9 at 1.0 Gyr. The subducted oceanic crust includes an internal heating of 20 in this case.

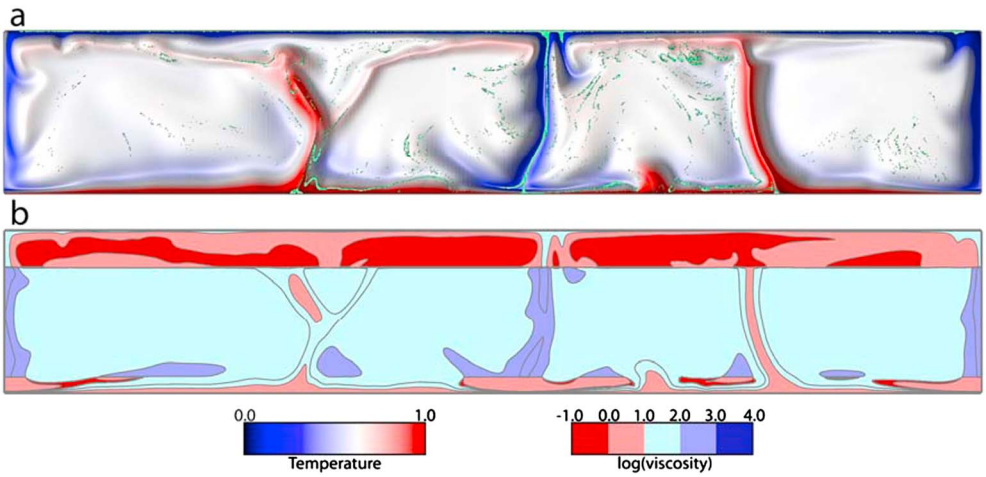

Figure 7. Case 10. (a) Snapshot (at 1.0 Gyr) of the nondimensional temperature and oceanic crust. (b) Logarithm of nondimensional viscosity at 1.0 Gyr. The black lines are contours of viscosity with an interval of 0.5. The viscosity is reduced by 100× in post-Perovskite regions.

the thin ribbon of oceanic crust within the downwelling region. The relatively undisturbed crust descends with the downwelling, without being stirred into the surrounding mantle. Once the crust reaches the lowermost mantle, along with the downwelling, it begins to migrate laterally toward one of the plume regions. Although the oceanic crust is denser than the surrounding mantle, most of it is unable to escape the viscous drag and settle to the lowermost mantle. Once it reaches a plume, it is viscously stirred into the background mantle. Several convection transit times have occurred by this time, and the mantle is littered with remnants of older crust that had been previously stirred by mantle plumes and is now being stirred by larger-scale mantle convection flow. The logarithm of the viscosity field at this time is shown in Figure 1b. Figures 1c and 1d show similar results at 2.0 and 2.8 billion years. At any given time, a small fraction of oceanic crust may reside in a tiny pile in the lowermost 0–200 km of a mantle plume, but this amount is variable and does not grow with time; it is continually entrained into the mantle plume itself. Figures 1e–1g show the depth profiles of average temperature, viscosity, and velocity magnitude, respectively.

[22] Case 2 employs a lower-density crust, with a buoyancy number of 0.6. Snapshots in time are shown at 1.0 and 2.8 billion years in Figures 2a and 2b, respectively. The results are very similar to that of Case 1, with the main difference being that small piles of oceanic crust do not form at the base of mantle plumes in this lower-density case. Case 3 employs a higher-density crust, with a buoyancy number of 1.0. Snapshots at 1.0 and 2.8 billion years are shown in Figures 2c and 2d, respectively. The results are characteristically similar to that of Case 1, and we did not identify any noticeable differences from the reference case.

[23] In Case 4, the buoyancy number of the oceanic crust is increased to 1.2. Snapshots in time are shown at 1.0 and 2.8 billion years in Figures 3a and 3b, respectively. The results are quite similar to that of Case 1, with the main difference being that only a slightly larger fraction of oceanic crust resides at the base of plumes. However, this amount does not grow with time. In fact, there is a smaller accumulation of crust at the CMB at 2.8 billion years (Figure 3a) than at 1.0 billion years (Figure 3b). In Case 5, the density of the oceanic crust is further increased, with a buoyancy number of 1.5. Snapshots in time are shown at 1.0 and 2.8 billion years in Figures 3c and 3d, respectively. In this case, we see an increased amount of oceanic crust resides at the base of plumes. However, the majority of the subducted oceanic crust is still entrained up by plumes. At any given time, the piles are quite small compared to the size of LLSVPs, which extend vertically over 1000 km above CMB [*Wang and Wen*, 2007; *He and Wen*, 2009; *He and Wen*, 2012]. From Case 1 to Case 5, we find that the fraction of oceanic crust that accumulates at the CMB increases with the density of oceanic crust. However, none of these cases generates large accumulations of oceanic crust at the CMB at the scale of LLSVPs.

[24] Case 6 employs a lower Rayleigh number $Ra = 5.0 \times 10^6$. The combined temperature and composition field is shown in Figure 4a. In this case, two stable plumes form at the CMB which consistently entrain the subducted oceanic crust. Case 7 employs a higher Rayleigh number $Ra = 5.0 \times 10^7$. The combined temperature and composition field is shown in Figure 4b. The higher Rayleigh number leads to a more vigorous convection. The subducted oceanic crust experiences more vigorous entrainment into upwelling plumes and is difficult to accumulate into large piles at the CMB.

[25] Case 8 employs a higher temperature dependence of viscosity, such that the temperature-dependent viscosity contrast between the hottest and coldest regions is 10,000×. The combined temperature and composition field and the logarithm of viscosity at 1.0 billion years are shown in Figures 5a and 5b, respectively. We found two notable differences between this case and the reference case. Case 8 lacked the small piles of oceanic crust at the base of mantle plumes, and the oceanic crust was more efficiently stirred into the background mantle. Lowered viscosity in the high-temperature regions led to weaker and more vigorously advecting mantle plumes. Oceanic crust was unable to accumulate at the base of plumes due to more vigorous entrainment into the plume conduit. Furthermore, the decreased viscosity in the upper mantle promoted more rapid stirring there, and oceanic crust that returned to the upper mantle

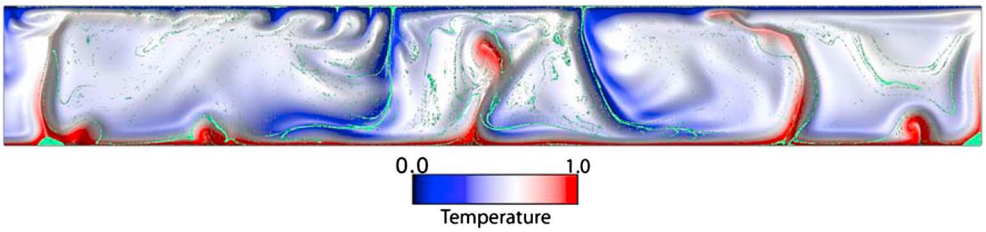

Figure 8. Snapshot of the nondimensional temperature and oceanic crust for Case 11 at 1.3 Gyr. The aspect ratio is 7 in this case.

via plume upwelling and return flow was promptly and efficiently stirred into the background mantle.

[26] In Case 9, the subducted oceanic crust includes an internal heating of $Q_{crust} = 20$. Figure 6 shows the combined temperature and composition field for Case 9 at 1.0 billion years. The results are very similar to that of Case 1. We did not identify noticeable differences from the reference case.

[27] In Case 10, we investigated the potential softening of downwelling material due to the Perovskite to post-Perovskite phase change [e.g., *Hunt et al*., 2009; *Ammann et al*., 2010]. Because the post-Perovskite transition is expected to occur in higher-pressure, colder regions of the mantle, it should be mostly present in the lowermost mantle portion of downwellings. In this case, we imposed a 100× viscosity reduction in regions of post-Perovskite phase transition. The combined temperature and composition field and the logarithm of viscosity are shown in Figures 7a and 7b, respectively, at 1 billion years of model time. Note the lowered viscosity at the base of downwelling regions. The lowered viscosity at the base of the downwelling region allows oceanic crust to migrate deeper, into the lower thermal boundary layer above the bottom boundary (i.e., core-mantle boundary). However, the crust is still easily entrained up by upwelling plumes.

[28] In Case 11, we employ an aspect ratio of 7 for the model. Figure 8 shows the combined temperature and composition field for Case 11 at 1.3 billion years. This case is featured by two downwellings on both sides of one upwelling plume in the center of the model. Although approximately twice the amount of oceanic crust comes into interaction with this plume compared to previous cases, the subducted oceanic crust is still entrained into this plume, and no crustal material resides at the base of the plume. Small piles exist at the base of the plumes at/near the side boundaries. However, these piles could be more influenced by boundary conditions and are not representative.

4. Discussion and Conclusion

[29] We investigated whether the negative buoyancy associated with subducted oceanic crust can overcome the viscous forces associated with mantle plumes and accumulate into large thermochemical piles with the same size as LLSVPs. In the cases presented here, we varied the density of oceanic crust relative to the surrounding mantle, the temperature dependence of viscosity, the Rayleigh number, the internal heating of subducted oceanic crust, and a potential weakening of slab regions due to a rheological weakening from the post-Perovskite phase transition. We also explore the influences of different aspect ratios of the model. We found that viscous stirring caused by mantle plumes was stronger than the negative buoyancy of oceanic crust, and the majority of the subducted oceanic crust was stirred into the surrounding mantle. For some cases, a small amount of oceanic crust formed small, narrow piles on the order of hundreds of kilometers or less in height at the base of mantle plumes. This material was subsequently entrained into plumes at a rate equal to or exceeding the rate at which it could accumulate. Even though the buoyancy number of subducted oceanic crust is increased to 1.5, it is still difficult to accumulate into large piles at the CMB with the same scale as LLSVPs. Our results are consistent with that of *Deschamps et al*. [2012] who show that seismic velocities of LLSVPs are better explained by iron and silicate-rich primordial materials than subducted oceanic crust.

[30] Our cases assumed a crustal thickness and a density that remained constant, at present-day values, over billions of years. If oceanic crust was thicker or denser in the geologic past, it would have stronger negative buoyancy and could therefore accumulate into large thermochemical structures in the lowermost mantle. For example, *Brandenburg and van Keken* [2007] found that if oceanic crust has a density higher than that inferred from experimental results, significant accumulation of crust could occur. This also occurs in calculations in which the oceanic crust is significantly thicker than present-day values [e.g., *Nakagawa et al*., 2009]. Furthermore, warmer mantle temperatures associated with earlier geologic times could facilitate temporary storage of oceanic crust in the transition zone that could episodically avalanche into the lower mantle, enhancing accumulation within the lower mantle [e.g., *Davies*, 2008]. Therefore, it is possible that different conditions associated with early Earth history may have promoted the accumulation of oceanic crust.

[31] We found that weakened post-Perovskite facilitated segregation of oceanic crust, allowing it to reach the lowermost thermal boundary layer, consistent with that of *Nakagawa and Tackley* [2011]. However, their study found that weakened post-Perovskite increased the amount of accumulation, whereas we find that once the oceanic crust reaches the lowermost thermal boundary, it is sheared and stretched, becoming even thinner and more easily stirred and entrained into mantle plumes. The thickness of the crust in *Nakagawa and Tackley* [2011] is unclear because they employ a melt algorithm to generate the crust, which may lead to thicker crust at earlier times.

[32] We allow downwellings to form self-consistently, which results in symmetric subduction. As a result, our effective crustal thickness in the downwelling varies up to twice the crustal thickness (we measured a representative

snapshot to be ~9 km thick at the top of the lower mantle). In order to keep the mesh resolution in the lowermost mantle at least as fine as the crustal thickness, we did not explore thinner crust. From our preliminary calculations and other studies [e.g., *Nakagawa et al*., 2009], we found that the amount of long-term crustal accumulation at the base of the mantle increases with greater crustal thickness. Therefore, our results likely represent an upper bound, and thinner crust would be more easily stirred by and entrained into mantle plumes. Alternatively, we explored using kinematic boundary conditions at the surface which generated asymmetric subduction, but we were unable to find a satisfactory configuration that prevented downwellings from unnaturally deflecting in an artificial, kinematically induced mantle wind. *Tackley* [2011] reproduced asymmetric subduction by imposing a slab in a uniform, nonconvecting mantle as the initial condition. In some cases, the descending lithosphere and crust flipped upside down, allowing the crust to come into contact with the lowermost thermal boundary layer (not being impeded by the lithosphere), allowing it to be more easily segregated, especially in 3-D calculations. It is unclear how to compare this study to ours, in terms of the amount of crustal accumulation. In *Tackley* [2011], plumes form in response to the slab contacting the CMB, whereas in our calculations, oceanic crust is swept toward preexisting plumes within upwelling regions. Furthermore, in *Tackley* [2011], the oceanic crust is prescribed to be 30 km thick because of presumed thickening as a slab passes through a viscosity increase at the top of the upper mantle. Our calculations employ a 50× viscosity increase; however, we find that the crust does not thicken when passing into higher-viscosity lower mantle. Some previous studies on viscous mixing show that mixing in 3-D is as efficient as that in 2-D [*Coltice and Schmalzl*, 2006; *Ferrachat and Ricard*, 1998]. This implies that there should not be large difference between 2-D and 3-D calculations in terms of the amount of crustal material that can accumulate in upwelling regions.

[33] In Case 1 and Case 8, we investigated changing the temperature dependence of viscosity from 1000× (Case 1) to 10,000× (Case 8). We found that increasing the temperature dependence of viscosity did not cause an increase in accumulation of oceanic crust at the CMB. At first glance, this appears to contradict to *Christensen and Hofmann* [1994], who found that the amount of crust segregation increases with the degree of temperature dependence of viscosity. Therefore, we performed additional cases with temperature-dependent viscosity in the range of isoviscous to 10,000× viscosity contrast due to temperature. Like *Christensen and Hofmann* [1994], we found that the amount of oceanic crust accumulating at the CMB roughly increases with the degree of temperature dependence of viscosity. However, in all cases, the amount of accumulation remains small. After more detailed comparison between Case 1 and Case 8, we found that a higher degree of temperature dependence of viscosity leads to higher viscosity contrast around the top of downwelling regions. This leads to larger velocity gradient in these regions where oceanic crust is more stretched and becomes slightly thinner (about 1 km thinner). Therefore, to first order, the amount of crustal accumulation at the CMB should increase with the degree of temperature dependence of viscosity; however, our results show that even a slight reduction of crustal thickness can counteract the effects of increasing the temperature dependence of viscosity by a factor of 10.

[34] In summary, one hypothesis for the cause of LLSVPs is that they are thermochemical piles caused by accumulation of subducted oceanic crust at the CMB. However, although subducted oceanic crust is denser than its surroundings, it was unclear whether thin oceanic crust could provide enough negative buoyancy to overcome viscous stresses that act to stir the crust into the mantle. Our results find that viscous forces caused by mantle plume regions are stronger than the negative buoyancy of subducted oceanic crust, so the crust is easily stirred into the background mantle. A small amount of crustal material may collect at the base of plumes, but it is sufficiently entrained away into the plume and does not accumulate into larger-scale thermochemical structures. Therefore, it is difficult for the subducted oceanic crust to accumulate into large piles at the CMB with the same size as LLSVPs. Our study does not preclude accumulation of oceanic crust at earlier times in the Earth's history when oceanic crust may have been thicker and/or the early Earth's mantle facilitated storage and later avalanching of crust at the transition zone.

[35] **Acknowledgments.** We thank John Hernlund and Wei Leng for careful and insightful reviews. We thank Ed Garnero for constructive conversations. This work is supported by NSF grants EAR-0838565 and EAR-1045788.

References

Ammann, M. W. et al. (2010), First-principles constraints on diffusion in lower-mantle minerals and a weak D″ layer, *Nature*, *465*(7297), 462–465.

Brandenburg, J. P., and P. E. van Keken (2007), Deep storage of oceanic crust in a vigorously convecting mantle, *J. Geophys. Res.*, *112*, B06403, doi:10.1029/2007GC001692.

Buffett, B. A., E. J. Garnero, and R. Jeanloz (2000), Sediments at the top of Earth's core, *Science*, *290*(5495), 1338–1342.

Bunge, H. P. et al. (1998), Time scales and heterogeneous structure in geodynamic Earth models, *Science*, *280*(5360), 91–95.

Christensen, U. R., and A. W. Hofmann (1994), Segregation of subducted oceanic crust in the convecting mantle, *J. Geophys. Res.*, *99*(B10), 19867–19884, doi:10.1029/93JB03403.

Coltice, N., and J. Schmalzl (2006), Mixing times in the mantle of the early Earth derived from 2-D and 3-D numerical simulations of convection, *Geophys. Res. Lett.*, *33*, L23304, doi:10.1029/2006GL027707.

Davies, G. F. (2008), Episodic layering of the early mantle by the "basalt barrier" mechanism, *Earth Planet Sci. Lett.*, *275*(3-4), 382–392.

Deschamps, F. et al. (2012), The primitive nature of large low shear-wave velocity provinces, *Earth Planet Sci. Lett.*, *349–350*(0), 198–208.

Ferrachat, S., and Y. Ricard (1998), Regular vs, chaotic mantle mixing, *Earth Planet Sci. Lett.*, *155*(1-2), 75–86.

Ford, S. R., *et al*. (2006), A strong lateral shear velocity gradient and anisotropy heterogeneity in the lowermost mantle beneath the southern Pacific, *J. Geophys. Res.*, *111*, B03306, doi:10.1029/2004JB003574.

Garnero, E. J., and A. K. McNamara (2008), Structure and dynamics of Earth's lower mantle, *Science*, *320*(5876), 626–628.

Grand, S. P. (2002), Mantle shear-wave tomography and the fate of subducted slabs, *Phil. Trans. Roy. Soc. Lond. Series Math. Phy. Eng. Sci.*, *360*(1800), 2475–2491.

Grand, S. P. et al. (1997), Global seismic tomography: A snapshot of convection in the Earth, *GSA Today*, *7*, 1–7.

He, Y., and L. Wen (2009), Structural features and shear-velocity structure of the "Pacific anomaly", *J. Geophys. Res.*, *114*, B02309, doi:10.1029/2008JB005814.

He, Y., and L. Wen (2012), Geographic boundary of the "Pacific anomaly" and its geometry and transitional structure in the north, *J. Geophys. Res.*, *117*, B09308, doi:10.1029/2012JB009436.

Hernlund, J. W., and C. Houser (2008), The statistical distribution of seismic velocities in Earth's deep mantle, *Earth Planet Sci. Lett.*, *265*(3-4), 423–437.

Hernlund, J. W. et al. (2005), A doubling of the post-Perovskite phase boundary and structure of the Earth's lowermost mantle, *Nature*, *434*(7035), 882–886.

van der Hilst, R. D. et al. (2007), Seismostratigraphy and thermal structure of Earth's core-mantle boundary region, *Science*, *315*(5820), 1813–1817.
Hirose, K. et al. (2005), Phase transition and density of subducted MORB crust in the lower mantle, *Earth Planet Sci. Lett.*, *237*(1-2), 239–251.
Huang, J., and G. F. Davies (2007), Stirring in three-dimensional mantle convection models and implications for geochemistry: 2. Heavy tracers, *Geochem. Geophys. Geosyst.*, *8*, Q07004, doi:10.1029/2007GC001621.
Hunt, S. A. et al. (2009), Weakening of calcium iridate during its transformation from Perovskite to post-Perovskite, *Nat. Geosci.*, *2*(11), 794–797.
Ishii, M., and J. Tromp (1999), Normal-mode and free-air gravity constraints on lateral variations in velocity and density of Earth's mantle, *Science*, *285*(5431), 1231–1236.
Kanda, R. V. S., and D. J. Stevenson (2006), Suction mechanism for iron entrainment into the lower mantle, *Geophys. Res. Lett.*, *33*, L02310, doi:10.1029/ 2005GL025009
Labrosse, S., J. W. Hernlund, and N. Coltice (2007), A crystallizing dense magma ocean at the base of the Earth's mantle, *Nature*, *450*(7171), 866–869.
Lee, C.-T. A., P. Luffi, T. Höink, J. Li, R. Dasgupta, and J. Hernlund (2010), Upside-down differentiation and generation of a "primordial" lower mantle, *Nature*, *463*(7283), 930–933.
Li, X. D., and B. Romanowicz (1996), Global mantle shear velocity model developed using nonlinear asymptotic coupling theory, *J. Geophys. Res.*, *101*(B10), 22245–22272, doi:10.1029/96JB01306.
Li, C., et al. (2008), A new global model for P wave speed variations in Earth's mantle, *Geochem. Geophys. Geosyst.*, *9*, Q05018, doi:10.1029/ 2007GC001806.
LithgowBertelloni, C., and M. Gurnis (1997), Cenozoic subsidence and uplift of continents from time-varying dynamic topography, *Geology*, *25*(8), 735–738.
Masters, G., G. Laske, H. Bolton, and A. M. Dziewonski (2000), The relative behavior of shear velocity, bulk sound speed, and compressional velocity in the mantle: implications for chemical and thermal structure, in *Earth's Deep Interior: Mineral Physics and Tomography From the Atomic to the Global Scale*, edited by S. Karato, et al., pp. 63–86, AGU, Washington, D.C.
McNamara, A. K., and S. Zhong (2005), Thermochemical structures beneath Africa and the Pacific Ocean, *Nature*, *437*(7062), 1136–1139.
Moresi, L., and M. Gurnis (1996), Constraints on the lateral strength of slabs from three-dimensional dynamic flow models, *Earth Planet Sci. Lett.*, *138*(1-4), 15–28.
Moresi, L. N., and V. S. Solomatov (1995), Numerical investigation of 2D convection with extremely large viscosity variations, *Physics of Fluids*, *7*(9), 2154–2162.
Murakami, M. et al. (2004), Post-Perovskite phase transition in MgSiO3, *Science*, *304*(5672), 855–858.
Nakagawa, T., and P. J. Tackley (2011), Effects of low-viscosity post-Perovskite on thermo-chemical mantle convection in a 3-D spherical shell, *Geophys. Res. Lett.*, *38*, L04309, doi:10.1029/2010GL046494.
Nakagawa, T., et al. (2009), Incorporating self-consistently calculated mineral physics into thermochemical mantle convection simulations in a 3-D spherical shell and its influence on seismic anomalies in Earth's mantle, *Geochem. Geophys. Geosyst.*, *10*, Q03004, doi:10.1029/2008GC002280.
Ni, S., and D. V. Helmberger (2003), Ridge-like lower mantle structure beneath South Africa, *J. Geophys. Res.*, *108*(B2), 2094, doi:10.1029/ 2001JB001545.
Ni, S. *et al*. (2002), Sharp sides to the African superplume, *Science*, *296*(5574), 1850–1852.
Nomura, R., H. Ozawa, S. Tateno, K. Hirose, J. Hernlund, S. Muto, H. Ishii, and N. Hiraoka (2011), Spin crossover and iron-rich silicate melt in the Earth's deep mantle, *Nature*, *473*(7346), 199–202.
O'Farrell, K. A., and J. P. Lowman (2010), Emulating the thermal structure of spherical shell convection in plane-layer geometry mantle convection models, *Phys. Earth Planet. In.*, *182*(1-2), 73–84.
Oganov, A. R., and S. Ono (2004), Theoretical and experimental evidence for a post-Perovskite phase of MgSiO3 in Earth's D″ layer, *Nature*, *430*(6998), 445–448.
Ricolleau, A., *et al*. (2010), Phase relations and equation of state of a natural MORB: Implications for the density profile of subducted oceanic crust in the Earth's lower mantle, *J. Geophys. Res.*, *115*, B08202, doi:10.1029/ 2009JB006709.
Ringwood, A. E. (1990), Slab-mantle interactions.3. Petrogenesis of intraplate magmas and structure of the upper mantle, *Chem. Geol.*, *82*(3-4), 187–207.
Ritsema, J., et al. (2004), Global transition zone tomography, *J. Geophys. Res.*, *109*, B02302, doi:10.1029/2003JB002610.
Su, W. J., and A. M. Dziewonski (1997), Simultaneous inversion for 3-D variations in shear and bulk velocity in the mantle, *Phys. Earth Planet. In.*, *100*(1-4), 135–156.
Tackley, P. J. (2011), Living dead slabs in 3-D: The dynamics of compositionally-stratified slabs entering a "slab graveyard" above the core-mantle boundary, *Phys. Earth Planet. In.*, *188*(3-4), 150–162.
Tackley, P. J. (2012), Dynamics and evolution of the deep mantle resulting from thermal, chemical, phase and melting effects, *Earth-Sci. Rev.*, *110*(1-4), 1–25.
Tackley, P. J., and S. D. King (2003), Testing the tracer ratio method for modeling active compositional fields in mantle convection simulations, *Geochem. Geophys. Geosyst.*, *4*(4), 8302, doi:10.1029/2001GC000214.
To, A. *et al*. (2005), 3D effects of sharp boundaries at the borders of the African and Pacific superplumes: Observation and modeling, *Earth Planet Sci. Lett.*, *233*(1-2), 137–153.
Torsvik, T. H. et al. (2010), Diamonds sampled by plumes from the core-mantle boundary, *Nature*, *466*(7304), 352–355.
Trampert, J. et al. (2004), Probabilistic tomography maps chemical heterogeneities throughout the lower mantle, *Science*, *306*(5697), 853–856.
Tsuchiya, T. et al. (2004), Phase transition in MgSiO3 Perovskite in the Earth's lower mantle, *Earth Planet Sci. Lett.*, *224*(3-4), 241–248.
Wang, Y., and L. Wen (2004), Mapping the geometry and geographic distribution of a very low velocity province at the base of the Earth's mantle, *J. Geophys. Res.*, *109*, B10305, doi:10.1029/2003JB002674.
Wang, Y., and L. X. Wen (2007), Geometry and P and S velocity structure of the "African anomaly", *J. Geophys. Res.*, *112*, B05313, doi:10.1029/ 2006JB004483.
Wen, L. X. (2001), Seismic evidence for a rapidly varying compositional anomaly at the base of the Earth's mantle beneath the Indian Ocean, *Earth Planet Sci. Lett.*, *194*(1-2), 83–95.
Wen, L., P. Silver, D. James, and R. Kuehnel (2001), Seismic evidence for a thermo-chemical boundary at the base of the Earth's mantle, *Earth Planet Sci. Lett.*, *189*(3-4), 141–153.
Zhong, S. et al. (2000), Role of temperature-dependent viscosity and surface plates in spherical shell models of mantle convection, *J. Geophys. Res.*, *105*(B5), 11063–11082, doi:10.1029/2000JB900003.